Oxygen content variation and cation doping dependence of $(La)_{1.4}(Sr_{1-y}Ca_y)_{1.6}Mn_2O_{7\pm\delta}$ ($y=0, 0.25, 0.5$) bilayered manganites

Lorenzo Malavasi,[1,*] Maria Cristina Mozzati,[2] Cristina Tealdi,[1] Carlo B. Azzoni,[2] and Giorgio Flor[1]
[1]*Dipartimento di Chimica Fisica "M. Rolla," INSTM, IENI/CNR Unità di Pavia of Università di Pavia, V. le Taramelli 16, I-27100 Pavia, Italy*
[2]*CNISM, Unità di Pavia and Dipartimento di Fisica "A. Volta," Università di Pavia, Via Bassi 6, I-27100 Pavia, Italy*
(Received 24 March 2006; published 8 August 2006)

The results of the synthesis and characterization of the *optimally* doped $(La)_{1.4}(Sr_{1-y}Ca_y)_{1.6}Mn_2O_{7\pm\delta}$ solid solution with $y=0$, 0.25, and 0.5 are reported. By progressively replacing the Sr with the smaller Ca, while keeping fixed the hole concentration due to the divalent dopant, the "size effect" of the cation itself on the structural, transport, and magnetic properties of the bilayered manganite has been analyzed. Two different annealing treatments of the solid solution, in pure oxygen and in pure argon, allowed us to also study the effect of the oxygen content variation. Structure and electronic properties of the samples have been investigated by means of x-ray powder diffraction and x-ray absorption spectroscopy measurements. Magnetoresistivity and static magnetization measurements have been carried out to complete the samples characterization. Oxygen annealing of the solid solution, which showed a limit for $y\sim0.5$, induces an increase of the Mn average valence state and a transition of the crystal structure from tetragonal to orthorhombic while the argon annealing induces an oxygen understoichiometry and, in turn, a reduction of the Mn average valence state. Along with the Ca substitution, the Jahn-Teller distortion of the MnO_6 octahedra is reduced. This has been directly connected to a general enhancement of the transport properties induced by the Ca doping. For the same cation composition, oxygen overstoichiometry leads to higher metal-insulator transition temperatures and lower resistivity values. Curie temperatures (T_C) are reduced by increasing the Ca doping. The lower T_C for all the annealed samples with respect to the as-prepared ones are connected to the strong influence on the magnetic interactions of the point defects due to the δ-variation.

DOI: 10.1103/PhysRevB.74.064104 PACS number(s): 75.47.Lx, 61.10.Ht, 61.72.Ji

I. INTRODUCTION

Perovskite manganites represent nowadays one of the most intensively studied research topic in the fields of solid state chemistry and physics. This is due to several reasons, among which the high negative magnetoresistive effect, termed colossal (CMR), and the virtual infinite tunability of the physical properties of the $R_{1-x}A_xMnO_3$ perovskite structure by means of cation doping and/or oxygen content control.[1–8]

More recently, the discovery of the CMR effect in the $La_{2-2x}Sr_{1+2x}Mn_2O_7$ manganite, which represents the $n=2$ member of the Ruddlesden-Popper (R-P) series of manganites, has attracted special interest due to its crystal structure forming a naturally layered system.[9–13] In particular, distinct features of the bilayered manganites are the anisotropic characteristics in both charge-transport and magnetic properties and the reduced dimensionality of the Mn-O-Mn networks, which lead to several intriguing changes including enhanced MR effects, large magnetocaloric effects, unconventional magnetostriction, and anisotropic transport in charge carriers. Moreover, these layered systems exhibit a variety of both ferromagnetic and antiferromagnetic structures.

The generic formula of the R-P phases is $A_{n+1}Mn_nO_{3n+1}$ which corresponds to the staggering of n perovskite layers intercalated by a rocksalt block. For $n=\infty$ the perovskite manganites are obtained while for $n=1$ the antiferromagnetic (AF) or spin-glass insulator phases $La_{1-x}Sr_{1+x}MnO_4$ are known.[14,15]

In the $n=2$ member $La_{2-2x}Sr_{1+2x}Mn_2O_7$ an extremely rich variety of magnetic phases have been found as a function of the Sr doping. One of the most interesting regions extends from $x=0.3$ to $x=0.4$ where ferromagnetic metals (FMM) are found. However, also within a relatively narrow doping range, several different kinds of arrangements of manganese ion spin occur. A common property is the presence of a two-dimensional (2D) ferromagnetic ordering in each perovskite layer and between the MnO_2 layers even though with different spin directions as a function of x. At $x=0.3$, the magnetic moments of each MnO_2 layer couple ferromagnetically within a bilayer and antiferromagnetically along the c axis, between successive bilayers. At $x\approx0.32$ the inter-bilayer coupling becomes FM but still directed along the c axis. At $x\geq0.33$ the magnetic moments direct along the ab plane. The magnetic coupling between the constituents single MnO_2 layers changes from FM into canted AF beyond $x\sim0.4$.[15] Also the magnetic coupling above the transition temperature (T_C) is rather interesting. As suggested by several groups,[16,17] a 2D ferromagnetic coupling within the plane should occur and the presence of a FM-AFM correlation between each plane in the bilayer unit, for $x=0.4$, has been pointed out. In any case, there exists two-dimensional ferromagnetic short-range order in a wide temperature region above T_C, which may be related to the anisotropic exchange energy ($|J_{ab}|>J_c|\gg||J'|$, J_{ab}, J_c, and J' standing for the in-plane, inter-single-layer, and inter-bilayer exchange interaction, respectively) in the quasi-two-dimensional FM system.

As in the perovskite manganites, a close coupling between the magnetic and transport properties is observed. However, due to the strong anisotropy that characterizes these layered systems, peculiar features have been observed.

Always considering the $0.3 \leq x \leq 0.4$ range for $La_{2-2x}Sr_{1+2x}Mn_2O_7$, single-crystal studies have shown that the ratio between the resistivity along the c axis (ρc) and the resistivity in the ab plane (ρ_{ab}) is as large as 10^2 at room temperature (RT), which suggests a confinement of the carrier motion within the MnO_2 bilayer. Usually, the onset of the long-range FM order is accompanied by a resistivity drop (the insulator-to-metal transition, IM) followed by a metallic-like transport. In the T range above T_C, both ρ_c and ρ_{ab} show an activated-like transport for $x=0.4$ with hopping energies around 30–40 meV.[18] By lowering the doping, the nature of the insulating state in the ρ_{ab} is progressively suppressed and, at $x=0.3$, a metallic-like transport ($d\rho_{ab}/dT>0$) is observed in the range $T_C \leq T \leq 270$ K.[9]

The doping-level dependence of the crystal structure of the bilayered manganites has been the object of several studies.[19–21] All the members of the $La_{2-2x}Sr_{1+2x}Mn_2O_7$ solid solution, for $0.3 \leq x \leq 0.5$, possess, at RT, a tetragonal structure belonging to the space group $I4/mmm$.

In particular, it has been shown that the $a(b)$ lattice parameter slightly increases with the increase of x, whereas the c parameter decreases more rapidly.[21] The lattice parameters variation reflects changes in the bond lengths. Taking into account the relative trend of the three distinct Mn-O bond lengths versus x, it turned out that the collective Jahn-Teller (J-T) distortion increases by decreasing the x value. Since the reduction of the cation doping corresponds to e_g electron doping, the systematic change of the Mn-O bond lengths reflects the electron occupancy of the two e_g orbital states.[21] The significant expansion of the out-of-plane Mn-O(2) bond (the one not directly linked to the other perovskite layer) by lowering the Sr doping is consistent with a shift of electron density from the planar (x^2-y^2) to the axial $(3z^2-r^2)$ orbitals.

The role of A-site doping on the bilayered manganites properties has been studied as done in the case of the perovskite manganites. However, fewer dopants have been considered and for less extensive doping levels due not only to the fact that the field of bilayered manganites is relatively new with respect to that of the perovskites, but also due to less straightforward preparation routes.

Battle *et al.*[22] considered the effect of La replacement with several other lanthanides (keeping Sr as the divalent dopant) and concluded that the size of the cation strongly influences the stability of the R-P phase and the A cations distribution between the two available crystallographic sites. Smaller lanthanides showed a preference in occupying the rocksalt layer with respect to the perovskite block. Moreover, they pointed out that cation disorder in compounds with larger lanthanides is at the origin of a subtle phase separation into two $n=2$ R-P phases.[22]

Calcium doping on the A site has been the object of an early investigation by Asano *et al.* who studied the $La_{2-2x}Ca_{1+2x}Mn_2O_7$ solid solution for $0 \leq x \leq 0.5$.[23] The main conclusion of that work is the clear evidence of two distinct types of FM ordering, which possibly result from anisotropic exchange interactions. Moreover, the material, in the doping region $0.22 \leq x \leq 0.5$, undergoes two transitions from a paramagnetic insulator to a ferromagnetic insulator and finally to a ferromagnetic metal with decreasing temperature. A model considering the *intra-* and *inter*layer spin arrangement was proposed.

Taking into account the available literature regarding the synthesis and characterization of bilayered manganites, it appears that further work is needed. A fundamental issue that has been well recognized in the perovskite manganites is the role and control of oxygen stoichiometries on their physical and chemical properties. We have clearly showed that any variation in the oxygen stoichiometry (δ) with respect to the ideal value of 3 not only induces a change of the Mn valence state but strongly influences the manganite properties through the point defects connected to the δ variation, namely cation vacancies ($\delta>0$) or anion vacancies ($\delta<0$).[7,8,24,25] We remark here that the presence of oxygen overstoichiometry ($\delta>0$) is not properly accounted for in the formalism $LaMnO_{3+\delta}$ since it is well established that the extra oxygen is not of an interstitial type but rather cation vacancies are formed for compensation.[25–27] So the correct formula for the oxygen overstoichiometric perovskites should be $La_{1-\epsilon}Mn_{1-\epsilon}O_3$, where $\epsilon=\delta/(3+\delta)$.

The role of oxygen content variation has never been systematically considered in any layered manganite (also encompassing the $n=1$ member of the R-P family). Only one thorough study by Milburn and Mitchell has recognized the importance of this topic in the $Nd_{2-2x}Sr_{1+2x}Mn_2O_7$ system ($0.10 \leq x \leq 0.70$), where they analyzed the phase diagram as a function of composition and oxygen partial pressure.[28] The authors also considered the distribution of oxygen vacancies and found a close relationship between the composition and Mn average oxidation state. However, the characterization of the samples was mainly structural and so a direct link with the physical properties was not given.

In this paper we present the result of the synthesis and characterization of the $(La)_{1.4}(Sr_{1-y}Ca_y)_{1.6}Mn_2O_{7\pm\delta}$ solid solution for $y=0$, 0.25, 0.5. We chose this composition since it represents an *optimal* doping analogous to the $x=0.3$ doping in the $La_{1-x}A^{2+}_xMnO_3$ perovskite manganites. In addition, keeping fixed the hole concentration due to the divalent cation, we changed its size by progressively replacing the Sr with the smaller Ca. The extent of this solid solution showed a limit for $y \sim 0.5$.[29] Finally, in order to vary the oxygen content, the samples underwent two different annealing treatments, i.e., in pure oxygen and pure argon.

Samples so prepared have been fully characterized by what concerns their structure, by means of x-ray powder diffraction (XRPD), and their electronic properties, by means of x-ray absorption spectroscopy (XAS) measurements, which were mainly used to determine the Mn valence state. Magnetoresistivity (MR) and static magnetization (M) measurements have been carried out to complete the samples characterization.

The aim of this paper is to show the effect of the oxygen content variation and a possible "size effect" of the divalent A cation on the structural, transport, and magnetic properties of an optimally doped bilayered manganite.

II. EXPERIMENT

$(La)_{1.4}(Sr_{1-y}Ca_y)_{1.6}Mn_2O_{7\pm\delta}$ samples with $y=0$, 0.25, and 0.50 were synthesized by solid state reaction starting from

proper amounts of La_2O_3, Mn_2O_3, $SrCO_3$, and $CaCO_3$ (Aldrich >99.99%). Pellets were prepared from the thoroughly mixed powders and allowed to react first at 1273 K for 72 h and after at 1573 K for other 72 h. During these thermal treatments, the pellets were reground and repelletized at least three times. The as-prepared samples have been annealed in a homemade quartz apparatus at 1173 K and at $P(O_2) = 10^5$ Pa (pure oxygen) and 10^{-1} Pa (argon) for 48 h and cooled down to RT at 20 K/min.

XRPD patterns were acquired on a Bruker D8 Advance diffractometer equipped with a Cu anode, graphite monochromator on the diffracted beam, and proportional detector. Measurements were carried out in the angular range from 10° to 120° with a step size of 0.02° and a counting time of 10 s per step. Diffraction patterns were refined by means of Rietveld method with the FULLPROF software.[30]

Magnetization measurements were carried out with a superconducting quantum interference device (SQUID) magnetometer by applying different magnetic fields (0–7 T) in the temperature range 2–320 K. MR measurements were carried out between 320 and 10 K at various fields with the dc four-electrode method by means of a specific probe directly inside the SQUID apparatus.

Mn-K edges XAS spectra were collected in transmission mode at RT at the BM-08 beam line (GILDA) of the ESRF laboratory (Grenoble, France) using ion chambers as detectors. For all the measurements, the samples were mixed with cellulose and pressed into pellets. The amount of sample in the pellets was adjusted to ensure a total absorption (μ) above the edge around 2. Spectra were processed by subtracting the smooth pre-edge background fitted with a straight line. Each spectrum was then normalized to unit absorption at 1000 eV above the edge, where the extended x-ray absorption fine structure (EXAFS) oscillations were not visible any more. Spectra processing was done with the ATHENA software.[31] In all the measurements the spectrum of a metallic Mn foil was collected together with the spectra of the samples. This was done in order to give reliable data about the edge position.

III. RESULTS AND DISCUSSION

A. X-ray powder diffraction

Figure 1 reports the indexed diffraction pattern of the $La_{1.4}Sr_{1.6}Mn_2O_7$ manganite after the synthesis and prior to any thermal treatment [called in the following as-prepared (AP) samples] while a graphical representation of this structure is depicted in Fig. 2. The pattern can be perfectly indexed according to a tetragonal unit cell belonging to the $I4/mmm$ space group (no. 139). Lattice constants for this sample are $a=b=3.8682(2)$ Å, $c=20.274(1)$ Å, and cell volume 303.359(3) Å^3. These values are also reported in Table I together with the lattice constants for the as-prepared $La_{1.4}Sr_{1.2}Ca_{0.4}Mn_2O_7$ and $La_{1.4}Sr_{0.8}Ca_{0.8}Mn_2O_7$ samples, which were indexed in the $I/4mmm$ space group, as well. The lattice constant trend shows a progressive and significant reduction of the c parameter as the Ca doping increases while the $a(b)$ parameter first decreases passing to the

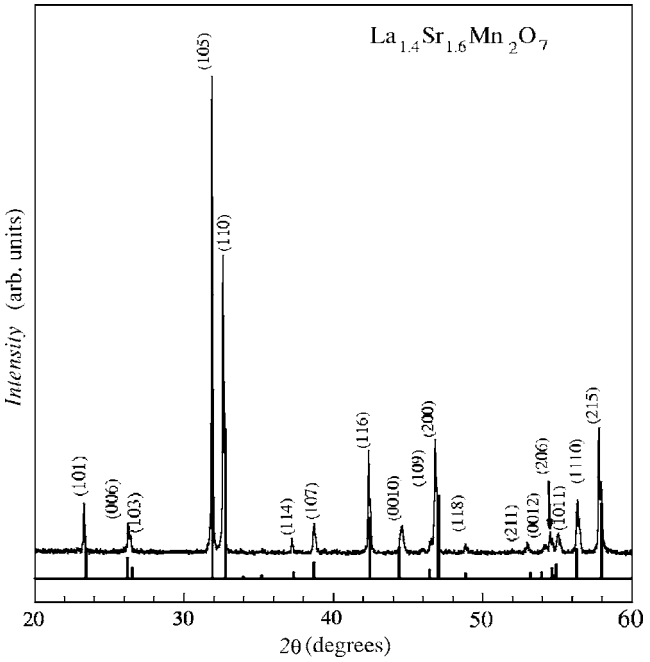

FIG. 1. X-ray diffraction pattern of the as-prepared (AP) $La_{1.4}Sr_{1.6}Mn_2O_7$ manganite. Bragg peaks appear as vertical gray lines.

$La_{1.4}Sr_{1.2}Ca_{0.4}Mn_2O_7$ composition and then increases when the Ca/Sr ratio is equal to 1. However, an overall reduction of the cell is found, as shown by the cell volume behavior. This is in agreement with the ionic radii difference between the Sr^{2+} and Ca^{2+} for the same coordination number, i.e., 1.40 and 1.26 Å, respectively.

Let us now pass to consider the effect of thermal annealing treatments on the samples. Figure 3 compares the XRPD patterns around the main peak for the $La_{1.4}Sr_{1.6}Mn_2O_7$ sample, chosen as a representative example, annealed in pure oxygen ("O annealed" in the figure) and pure argon ("Ar annealed" in the figure) with the as-prepared sample. From the patterns for the Ca undoped sample, it is clear that after the oxygen annealing a relevant broadening of the main peak located around 32° is observed. It passes from a full width at half maximum (FWHM) ~0.125° for the as-prepared sample to ~0.240° after the oxygen annealing, while the next peak, at about 32.5°, undergoes a reduced broadening from ~0.127° to ~0.143°. The first peak corresponds, in the tetragonal $I4/mmm$ structure, to the (105) diffraction line while the second one to the (110). The presence of this broadening, also found for other peaks in the pattern, may be indicative of a phase transition towards a less symmetric structure. As reported by Milburn and Mitchell[28] two distortions of the $I4/mmm$ cell to lower (orthorhombic) symmetry are known. The first one consists of a doubling of the cell size in a $(\sqrt{2}a)\times(\sqrt{2}b)\times c$ superstructure, with a rotation of 45° around the c parameter, in which the face diagonals of the $I4/mmm$ cell become the new cell vectors and the $\langle 100\rangle$ mirror planes are lost. When this distortion occurs, the tetragonal $\{hhl\}$ peaks split into $\{2h,0,l\}$ and $\{0,2h,l\}$, the tetragonal $\{hkl\}$ into $\{h+k,h-k,l\}$ and $\{h-k,h+k,l\}$ while the $\{h0l\}$ reflections remain unsplit. The second type of dis-

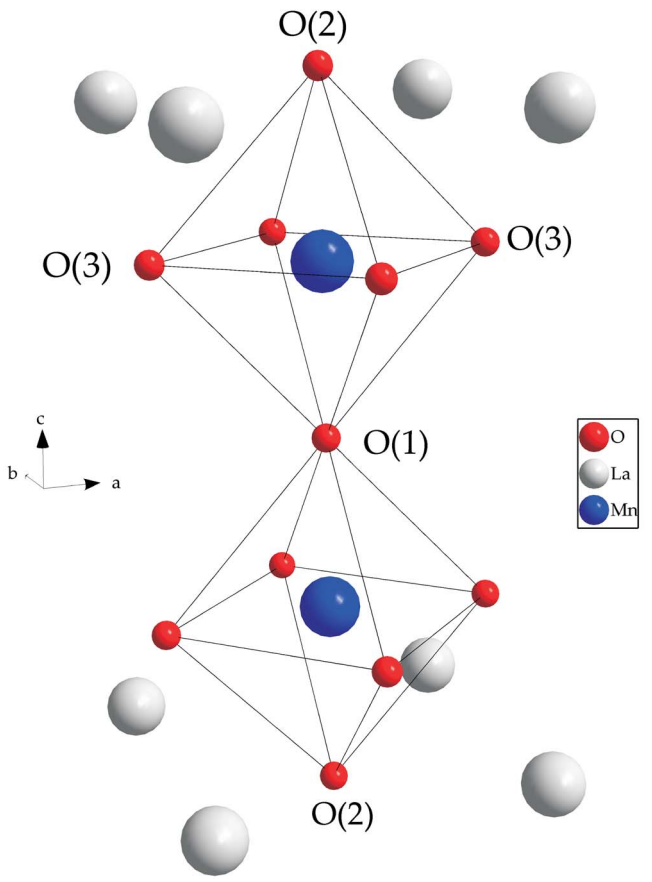

FIG. 2. (Color online) Sketch of the $I4/mmm$ crystal structure of the $La_{1.4}Sr_{1.6}Mn_2O_7$ manganite.

tortion involves the loss of the ⟨110⟩ mirror planes and gives origin to an orthorhombic cell of the same volume as the tetragonal one in which the a and b cell directions are no longer equivalent in magnitude. Such distortion has been reported for mixed valence compounds such as the K_2NiF_4-type nickelates[32,33] and for the $n=2$ layered manganites of the $Nd_{2-2x}Sr_{1+2x}Mn_2O_7$ system[28] where, however,

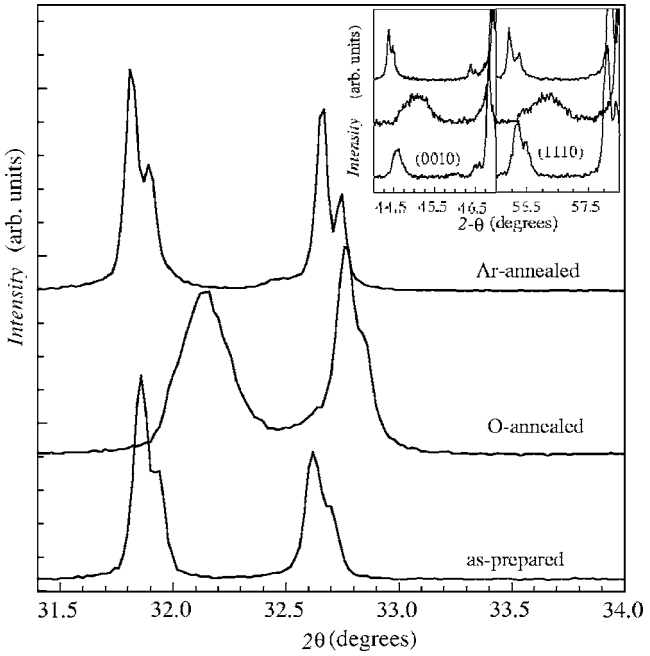

FIG. 3. XRPD patterns around the main peak for the AP, oxygen-annealed, and argon-annealed $La_{1.4}Sr_{1.6}Mn_2O_7$ samples. The inset shows, for the same patterns, the 2θ regions where the {0010} and {1110} reflections are located.

the orthorhombic transition was found for oxygen deficient samples ($\delta<0$) and not, as in the present case, for oxygen overstoichiometric ones ($\delta>0$). For this second distortion, the {hhl} reflections should remain degenerate whereas the {$h0l$} split into {$h0l$} and {$0hl$}. This structure is described in the *Immm* space group (no. 71).

By looking carefully through the XRPD patterns of the oxygen-annealed samples, we could observe the broadening of all the {$h0l$} reflections, thus confirming the occurrence of the second type of distortion. In fact, as shown by Fig. 3, the peak that corresponds to the single (105) reflection in the as-prepared sample, belonging to the $I4/mmm$ space group, has been split into two unresolved diffraction lines in the

TABLE I. Lattice constants (a, b, and c), cell volume (V), and c/a values for as-prepared (AP), oxygen (O) and argon (Ar) annealed $(La)_{1.4}(Sr_{1-y}Ca_y)_{1.6}Mn_2O_{7\pm\delta}$ ($y=0$, 0.25, and 0.50) samples.

Sample		a (Å)	B (Å)	c (Å)	V (Å^3)	c/a
$y=0$	AP	3.8682(2)	3.8682(2)	20.274(1)	303.3(3)	5.241(1)
$y=0.25$	AP	3.8640(1)	3.8640(1)	20.1366(7)	300.6(9)	5.211(3)
$y=0.50$	AP	3.8715(1)	3.8715(1)	19.8195(7)	297.0(2)	5.119(2)
$y=0$	O (62%)	3.8683(5)	3.8688(5)	20.175(3)	301.7(1)	5.215(3)
$y=0$	O (38%)	3.8666(6)	3.8698(7)	20.016(2)	299.4(2)	5.172(4)
$y=0.25$	O (60%)	3.8598(4)	3.8610(4)	19.880(2)	296.2(1)	5.149(3)
$y=0.25$	O (40%)	3.8601(4)	3.8618(5)	20.011(2)	298.3(1)	5.182(3)
$y=0.50$	O	3.8573(3)	3.8556(2)	19.693(1)	292.8(1)	5.105(2)
$y=0$	Ar	3.8635(1)	3.8635(1)	20.3576(6)	303.8(8)	5.269(1)
$y=0.25$	Ar	3.8642(1)	3.8640(1)	20.1953(8)	301.5(1)	5.226(1)
$y=0.50$	Ar	3.8696(4)	3.8696(4)	19.9810(8)	299.1(1)	5.164(3)

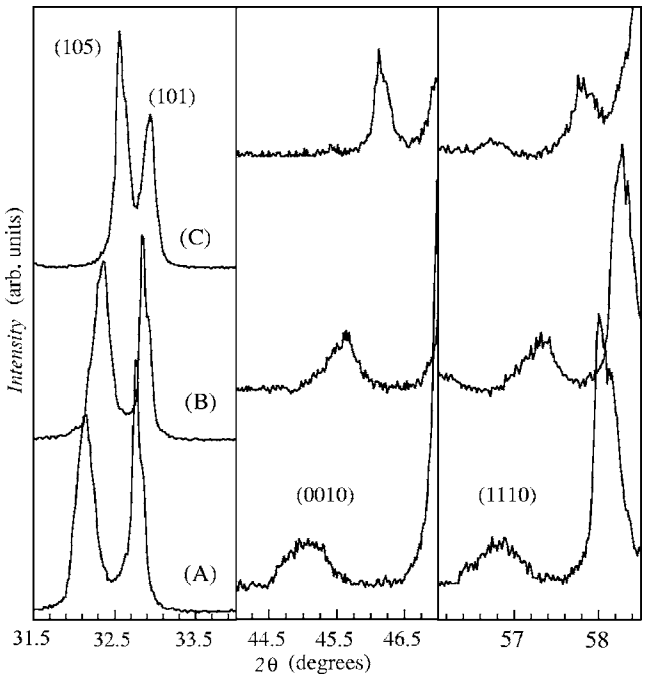

FIG. 4. XRPD patterns for the (a) $La_{1.4}Sr_{1.6}Mn_2O_7$, (b) $La_{1.4}Sr_{1.2}Ca_{0.4}Mn_2O_7$, and (c) $La_{1.4}Sr_{0.8}Ca_{0.8}Mn_2O_7$ samples annealed in pure oxygen (the same three 2θ regions of Fig. 3).

Immm symmetry, i.e., the (105) and (015) reflections. However, beside this evidence, some peaks belonging to the {*hhl*} type showed significant broadening, in particular for the {0010} and {1110} reflections, which should not be affected by the $I4/mmm \rightarrow Immm$ symmetry change. This is shown in detail in the inset of Fig. 3, which presents the 2θ regions where the {0010} and {1110} reflections are located, for the $La_{1.4}Sr_{1.6}Mn_2O_7$ as-prepared, oxygen-annealed, and argon-annealed samples.

However, this broadening effect has not the same extension for all the cation stoichiometries considered here. This is clearly shown in Fig. 4 where the same three regions of Fig. 3 are plotted for the $La_{1.4}Sr_{1.6}Mn_2O_7$, $La_{1.4}Sr_{1.2}Ca_{0.4}Mn_2O_7$, and $La_{1.4}Sr_{0.8}Ca_{0.8}Mn_2O_7$ samples annealed in pure oxygen. By increasing the Ca doping, the broadening of *all* the peaks, both belonging to the *Immm* symmetry and the other ones, are less broadened by the oxygen thermal treatment. For example, the FWHM for the as-prepared and oxygen-annealed $La_{1.4}Sr_{0.8}Ca_{0.8}Mn_2O_7$ sample is practically constant.

Let us consider now the strategy employed to treat the patterns of the samples annealed in pure oxygen. Regarding the Ca-undoped compound, a refinement with a single *Immm* phase did not lead to a good fit result ($R_B=12.1, \chi^2=5.04$). Several models were considered in order to improve the refinement. It was found that a better description of the experimental pattern could be achieved by means of a multiphase model. Also in this context, different combinations of tetragonal and orthorhombic phases were considered. An improvement of the data fit was obtained by means of a two *Immm*-phases model ($\chi^2=3.66$). This allowed a better description of most of the peaks but the ones indicated by significant broadening as the {0010} were not yet properly refined.

The results for $La_{1.4}Sr_{1.6}Mn_2O_7$ indicate the presence of about 62% of an orthorhombic phase with lattice constants $a=3.8688(5)$, $b=3.8683(5)$, and $c=20.175(3)$ and a second phase (about 38%) with lattice constants $a=3.8666(6)$, $b=3.8698(7)$, and $c=20.016(2)$. As can be noticed, the orthorhombic distortion is small for each phase and the main difference between them resides in the value of the parameter c. Probably, this difference arises from a difference in the relative occupancies of the A cations of the two available sites, i.e., in the perovskite or in the rocksalt layer, and/or also from an extremely small compositional difference between the two phases that could be related to a variation of the mean oxidation state of Mn ions.

Also for the $La_{1.4}Sr_{1.2}Ca_{0.4}Mn_2O_7$ sample, the agreement between the experimental and calculated patterns was achieved with a two-phase model, which resulted in a better fit with respect to the previous sample ($\chi^2=2.45$) and gave 60% of a phase with $a=3.8598(4)$, $b=3.8610(4)$, and $c=19.880(2)$ and about 40% of a second phase with $a=3.8618(5)$, $b=3.8601(4)$, and $c=20.011(2)$. For this sample and for the previous one, both sets of lattice constants are reported in Table I.

Finally, for the sample with an equal Sr/Ca ratio, the pattern refinement was reliable starting with a single-phase model. However, also in this case, the best agreement between the experimental and calculated patterns was achieved with an orthorhombic structure ($R_B=13.2$, $\chi^2=3.6$) instead of a tetragonal one ($R_B=19.6$, $\chi^2=5.7$). Lattice constants for this sample are listed in Table I, as well.

When the as-prepared samples have been annealed in pure argon the tetragonal structure has been preserved and no evidence of an anomalous broadening of any peak was detected. Again, in Table I, are reported all the lattice parameters for the argon-annealed $La_{1.4}Sr_{1.6}Mn_2O_7$, $La_{1.4}Sr_{1.2}Ca_{0.4}Mn_2O_7$, and $La_{1.4}Sr_{0.8}Ca_{0.8}Mn_2O_7$ samples.

Figure 5 summarizes the lattice constants variation by plotting the trend of cell volumes against the Ca content (y), thus referring to the formula $(La)_{1.4}(Sr_{1-y}Ca_y)_{1.6}Mn_2O_{7\pm\delta}$. Data are relative to the three cation compositions and to the as-prepared (white circles), oxidized (black triangles), and reduced (black squares) samples. According to the refinement results presented above, for the oxidized $La_{1.4}Sr_{1.6}Mn_2O_7$ and $La_{1.4}Sr_{1.2}Ca_{0.4}Mn_2O_7$, two values of the volume are reported in the figure.

For the same cation composition, the annealing treatment in pure oxygen induces a reduction of the cell volume with respect to the as-prepared samples. This links directly to the increase of the average oxidation state of Mn ions (being the ionic radii 0.645 Å and 0.53 Å for Mn^{3+} and Mn^{4+}, respectively[34]) as confirmed by the XAS results (see below). In addition, for $y=0$ and 0.25, this kind of treatment induces a phase separation in the samples giving origin to two distinct orthorhombic phases with similar a and b constants (differences lower than 0.1%) and more different c parameters ($\Delta c \sim 0.8-0.6\%$).

As suggested above, this phase separation is probably due to the effect of oxygen content increase. In three-dimensional (3D) perovskites such as $LaMnO_3$, it is well known that for $\delta>0$ the point defects compensations occur via cation vacancies formation according to[26]

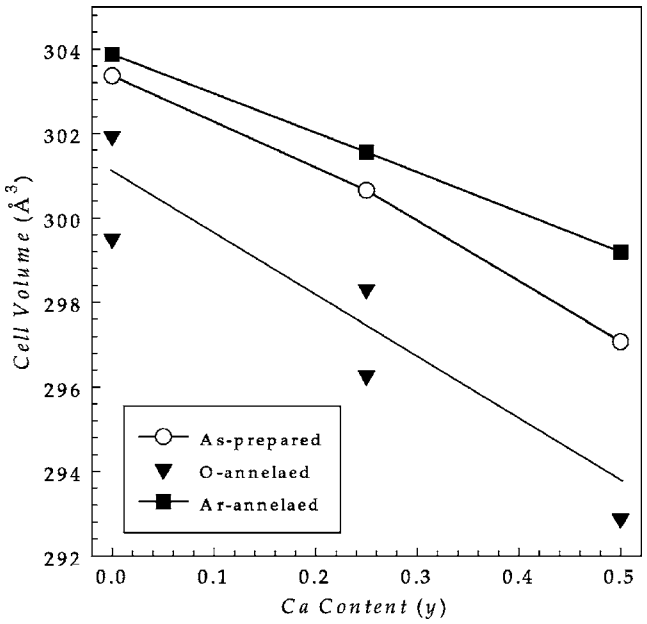

FIG. 5. Cell volumes against the Ca content (y), for the three cation compositions of the as-prepared (white circles), oxidized (black triangles), and reduced (black squares) samples.

$$\frac{1}{2}O_2 \underset{\leftarrow}{\rightarrow} O_O^x + \frac{1}{3}V_{La}''' + \frac{1}{3}V_{Mn}''' + 2h^{\bullet}. \quad (1)$$

The defect chemistry of 2D layered manganites has not been object of analogous studies apart from the (Nd,Sr)MnO system in presence of oxygen understoichiometry.[28] For oxygen overstoichiometric samples, we can just postulate the occurrence of a mechanism similar to that reported by Eq. (1) by considering, at a first approximation, that the perovskite layer, which is structurally analogous to the 3D perovskites, should behave in the similar way. In addition, also for the rocksalt layer, we can suppose that the oxygen overstoichiometry will be compensated by cation vacancies rather than oxygen interstitials as found in binary oxides with this crystal structure.[35]

The formation of cation vacancies may be at the base of the phase separation as a consequence of difference in their distribution and/or clustering phenomena. In particular, the actual distribution of cation vacancies may be not trivial since they can form on both the independent crystallographic sites corresponding to cations in the perovskite block, $2b(00\frac{1}{2})$, and in the rock-salt layer, $4e(00z)$. In addition, vacancies may prefer to localize on each site as a preference to create unequal numbers of cation vacancies, i.e., for example, again referring to Eq. (1), a ratio of $V_{La}'''/V_{Mn}''' \neq 1$, was found to occur in 3D perovskites.[25]

Opposite to the oxygen annealing, the treatment in pure argon, at fixed cation composition, induces an increase of the cell volumes for all the samples, as shown in Fig. 5. We remark here that the Vegards law is observed for all the monophasic sample series and that the solubility limit can be ruled out as the source of the aforementioned phase separation. Regarding the solubility limit of Ca in the $La_{1.4}Sr_{1.6}Mn_2O_7$ compound, we confirm the available literature results[29] which indicate a threshold around 0.5. In fact, any attempt to synthesize composition with a Ca/Sr ratio greater than 1 were unsuccessful. In all the cases, a perovskite phase together with SrO oxide were found to be the stable reaction products.

The cell volume increase found for the reduced samples can be connected to the reduction of the Mn sublattice as a consequence of the reduction of the oxygen content. This is in accordance with the XAS data (see later) which pointed out a Mn-edge shift towards lower energies for the argon-annealed samples with respect to the samples treated in pure oxygen.

Looking at the lattice constant trend of the argon-annealed samples, it is interesting to note an anisotropy in the lattice parameters variation, i.e., the progressive reduction of the c parameter and the increase of the in-plane parameters, which results in a progressive reduction of the c/a ratio. This result may be indicative of a variation in the Jahn-Teller distortion of the MnO_6 octahedra triggered by a variation in the nature of the orbital state of the e_g electrons where, for high Ca-content levels, the electrons prefer to occupy the $3x^2-y^2$ orbitals. This can be due to the effect of Ca doping on the electronic structure of the bilayered manganites. Even though the atomic position determined from the Rietveld refinement may not be fully reliable, particularly with reference to the oxygen atoms, the values of the Mn-O bond lengths have been used to determine the distortion of the octahedron by means of the Jahn-Teller parameter, defined as[13]

$$Q = 4\{(l+m)/2 - s\}, \quad (2)$$

where l, m, and s represent the long, medium, and short Mn-O bonds in the MnO_6 octahedron. By means of this expression, it is found that the Q value moves from 0.2952 to 0.2482 and finally to 0.1526 by increasing the Ca content. This result witnesses a reduction of the J-T distortion by increasing the Ca doping while keeping the overall hole content approximately constant.

B. X-ray absorption spectroscopy

XAS measurements at the Mn-K edge were carried out for the $La_{1.4}Sr_{1.6}Mn_2O_7$, $La_{1.4}Sr_{1.2}Ca_{0.4}Mn_2O_7$, and $La_{1.4}Sr_{0.8}Ca_{0.8}Mn_2O_7$ samples annealed in oxygen and argon. As a typical example, Fig. 6 reports the edge region spectra of the $La_{1.4}Sr_{1.6}Mn_2O_7$ sample annealed in pure oxygen ($La_{1.4}Sr_{1.6}Mn_2O_7$-O) and in pure argon ($La_{1.4}Sr_{1.6}Mn_2O_7$-Ar) together with the spectra of the two standards employed in this study: $LaMnO_3$ (Mn^{3+} standard) and $CaMnO_3$ (Mn^{4+} standard). A general view of the spectra of all the samples is presented in Fig. 7 with a vertical reference line passing through the maximum of the first sample.

The spectral line shapes and widths recorded are very similar for all the samples. A chemical shift of the threshold energies (E_0) (taken at the inflection point of the absorption edge) towards higher energies is found for the samples annealed in oxygen with respect to those annealed in argon, as shown clearly in Fig. 6 for $La_{1.4}Sr_{1.6}Mn_2O_7$. This chemical shift can be related to the increase of the average Mn va-

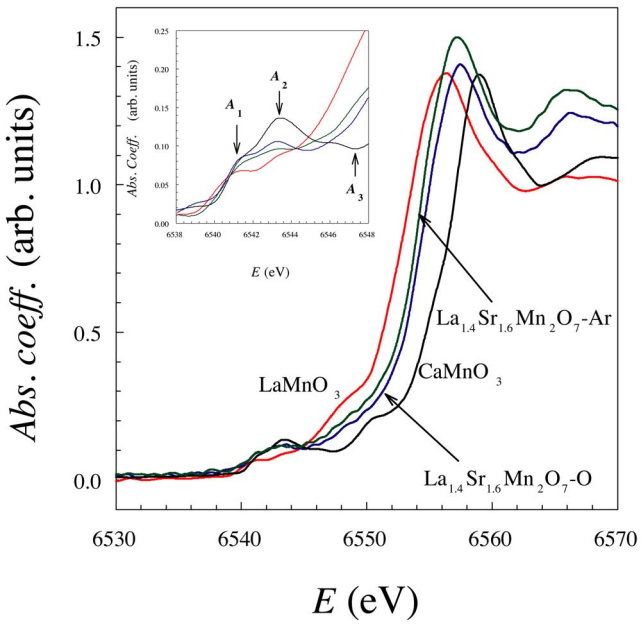

FIG. 6. (Color online) Edge region of the XAS spectra of the $La_{1.4}Sr_{1.6}Mn_2O_7$ samples: dotted line (blue) for the annealed in pure oxygen; long dashed (green) line for the annealed in pure argon; together with the spectra of the two standards: full line (red) for the $LaMnO_3$ and short dashed line (black) for the $CaMnO_3$. The inset shows an enlarged view of the low-energy part of the same spectra, evidencing the three features labeled as A_1, A_2, and A_3 on the $CaMnO_3$ spectrum (same symbols as the main figure).

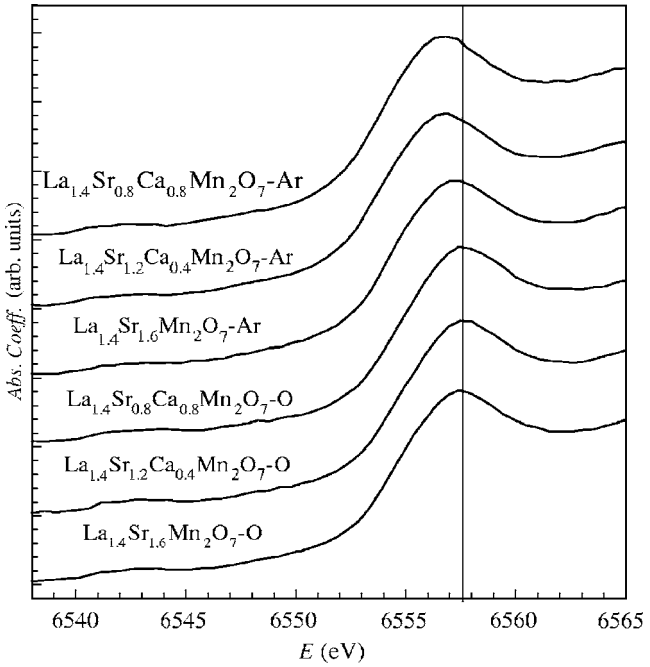

FIG. 7. General view of the XAS spectra of all the argon- and oxygen-annealed samples. The vertical line passing through the maximum of the oxygen-annealed $La_{1.4}Sr_{1.6}Mn_2O_7$ sample is drawn as reference.

lence, which is connected to the creation of holes in the rather localized d orbitals with consequent loss of screening.

The overall shift from +3 ($LaMnO_3$) to +4 ($CaMnO_3$) Mn valence was around 3.3 eV, in good agreement with previous available literature data.[36] Through the chemical shifts (ΔE_0), measured with respect to the $LaMnO_3$ threshold, and considering a roughly linear behavior of the edge position with the average Mn oxidation state[36,37] and our previous XAS data on 3D manganites,[38] we estimated the mean Mn valence state for each sample. We note that for the samples annealed in pure oxygen the Mn valence state is the same for the $y=0.25$ and 0.50 compositions ($\sim$3.38) and slightly lower for the Ca-undoped sample ($\sim$3.34). A significant reduction of the Mn valence state occurs after the argon annealing with estimated values of 3.27, 3.25, and 3.27 for the $y=0$, 0.25, and 0.5 samples, respectively. If one consider that an acceptable error on the valence evaluation through this procedure may be around 3–5%, also taking into account the data resolution, we note that the valence state within each of the two sample series may be thought to be nearly constant. This consideration will allow us to discern the influence of the divalent dopant on the physical properties of the samples considered.

Based on these results, the oxygen annealed samples possess an oxygen overstoichiometry (δ) of the order of 0.06 while those annealed in argon have an oxygen understoichiometry of about 0.04. This work considers primarily the role of oxygen stoichiometry fluctuations as the main variable to change the average Mn oxidation state of a bilayered manganites, where, usually, the hole doping is realized through the variation of the divalent dopant concentration.[10–13,36]

Some additional features of the XAS spectra can be noticed in the pre-edge region. The inset of Fig. 6 brings into prominence this part for the samples considered in that figure and indicates three features, labeled as A_1, A_2, and A_3, on the $CaMnO_3$ spectrum, due to their particular enhancement in this compound. These "peaks" have been correlated to the electronic and structural properties of the 3D manganites.[39,37] They originate from transitions to empty states with a d-like character ($1s \rightarrow 3d^{(n+1)}$). This kind of transition would be dipole forbidden; however, through an admixture of $3d$ and $4p$ states, it becomes weakly allowed. In addition, in the pre-edge region there is also some hybridization with the O $2p$ states. However, these considerations are not enough to account for the high intensity of these A_i features in samples such as the $CaMnO_3$ which presents Mn atoms at a point of inversion symmetry and nearly so even for the substituted $LaMnO_3$. A clarification of this point arose from the calculation of Elfimov[40] who showed that the $3d$ features correspond to a coupling of Mn $4p$ states with $3d$ states on adjacent Mn atoms. A more detailed description of these last aspects can be found in Refs. 36 and 39. Taking into account the calculation reported in the cited papers, it has been shown that the A_1 peak would correspond to transitions into empty majority-spin e_g states on the neighboring Mn ions and A_2 peak to transitions into the e_g and t_{2g} minority states. A more recent paper[41] suggests, as a further assumption, that the $1s$ to t_{2g} transition intensity vanishes as confirmed by theoretical calculations.[42,43]

Figures 8(a) and 8(b) put in prominence the pre-edge region for the oxygen and argon annealed samples, respec-

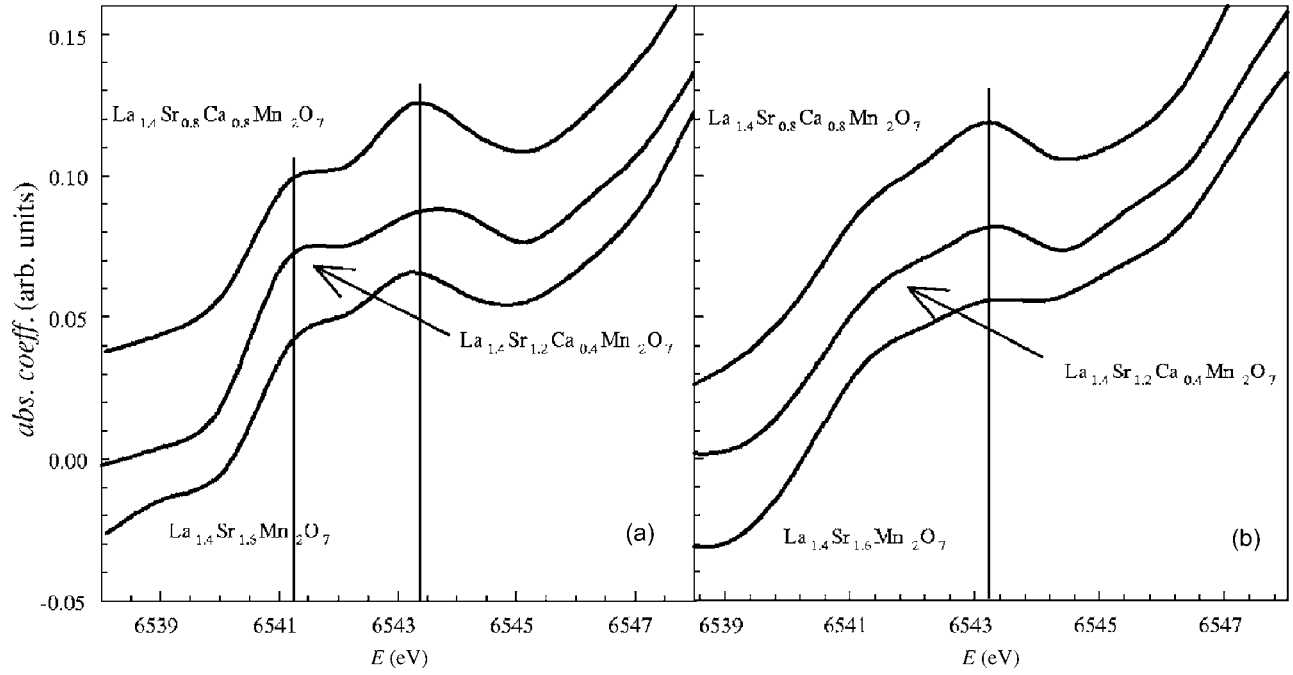

FIG. 8. Pre-edge region of the XAS spectra for the (a) oxygen- and (b) argon-annealed samples.

tively, by displaying the spectra in the range 6538–6548 eV. A deep analysis of these features goes beyond the scope of the present paper and will be the object of future work together with the analysis of the EXAFS signal; however, some general consideration of relevance for the following discussion may be done. First of all, the features that are found in the pre-edge region of the $n=\infty$ members of the R-P series (i.e., the 3D manganites), and which have been discussed above, are also observed for the $n=2$ members. In particular, just two A_i peaks (labeled A_1 and A_2) may be found in the spectra of our samples with a mean separation of about 2.1–2.2 eV in all the cases. The presence of just two peaks is in accordance with the observation that, in general, the A_3 peak is not observed in doped manganites also for high resolution data. No significant differences in the A_1–A_2 separation is found between the oxygen and argon annealed samples. Again, this is in agreement with the fact that a total decrease of the splitting of only ~0.3 eV is found when changing the average Mn valence from +3 to +4 (Ref. 36) and so the relatively small valence change between our samples should not strongly affect this aspect. Within each series, the position of the A_1 peak remains practically constant while some shift occurs for the A_2 peak. In particular, for the oxygen-annealed compounds, its position moves toward higher energy for the intermediate composition ($La_{1.4}Sr_{1.2}Ca_{0.4}Mn_2O_7$) and then shifts slightly back to lower energy for the Ca:Sr ratio equal to 1. Also for the reduced samples, the $La_{1.4}Sr_{1.2}Ca_{0.4}Mn_2O_7$ compound shows the A_2 peak at higher energy with respect to the other two stoichiometries.

Moreover, a significant difference in the relative intensity of the A_1 and A_2 peaks between samples annealed in different environment occurs; for the same composition, the oxygen treatment increases the intensity of both features. An increase of the A_1 peak intensity has been connected to an increase in the charge delocalization of the majority spin e_g^1 electron[44] and also to an enhancement of the covalent character, which can be connected to the increase in the oxygen content and in turn of the Mn valence state, which should broaden the conduction bandwidth.

Considering the two series separately, it can be noticed that there is a pronounced increase of the intensity of the A_2 feature as the Ca doping increases. As indicated above, this last peak should originate from transitions into e_g and (less) t_{2g} minority states. However, the reason of this enhancement may not be limited to this aspect. In fact, the $CaMnO_3$ (see inset of Fig. 6), differently from the pure $LaMnO_3$, shows a particularly intense A_2 peak. It has been pointed out by previous workers that the actually available models developed for describing the pre-edge features of manganites lack of some "ingredients," such as the (i) local distortions of the crystal and (ii) further change in covalency and hybridization. Since the average Mn valence state is approximately constant within each series of samples, it is clear that the enhancement of the A_2 feature must have another origin with respect to a simple change in the valence state. The main difference between the $LaMnO_3$ and $CaMnO_3$ spectra is the oxidation state change of Mn from +3 to +4; however, another significant difference is the absence of the Jahn-Teller distortion for the $CaMnO_3$ sample. What we propose is that the intensity of the A_2 peak is not only controlled by the average valence state but also by the J-T effect, i.e., by local distortions in the crystal structure. As a matter of fact, Fig. 9 presents the trend of bond lengths towards the Ca content for the argon-annealed samples (for the oxygen-annealed ones, the presence of two phases makes a schematization of the bond lengths trend not so meaningful). As can be appreciated, there is a progressive reduction of the difference between the Mn-O1 and Mn-O3 bonds as a function of y, which suggests a reduction of the J-T effect as the Ca doping

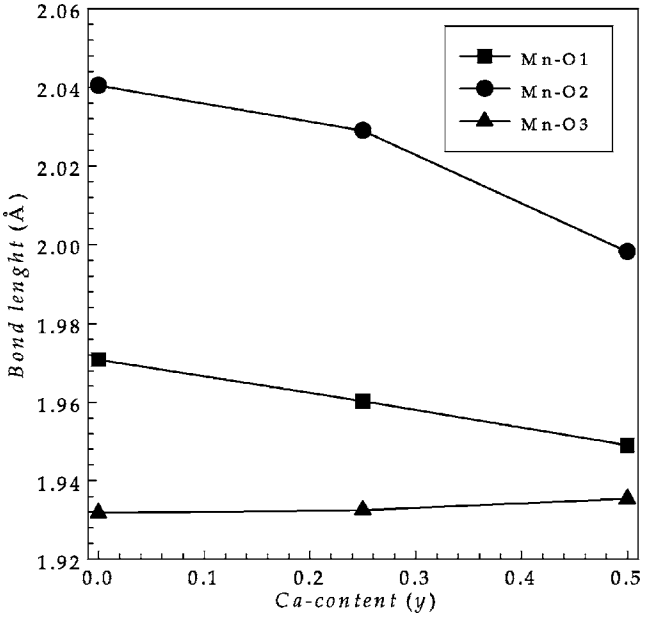

FIG. 9. Trend of the three Mn-O bond lengths towards the Ca-content (y) for the argon-annealed samples.

proceeds; this is also coupled to a general reduction of the distance between successive perovskite layers. However, we remark that the effect of this last evidence on the physical properties (such as the T_C) may be in competition with a reduction of the bandwidth as the mean ionic radius on the A site reduces and also with a reduction of the statistical variance in the distribution of ionic radii (σ^2).

C. Electrical conductivity and magnetoresistivity

Electrical conductivity measurements have been carried out on all the annealed samples at null applied magnetic field (H) and with a field of 1 and 7 T.

Figures 10 and 11 show the resistivity (ρ) curves for the $La_{1.4}Sr_{1.6}Mn_2O_7$ (a), $La_{1.4}Sr_{1.2}Ca_{0.4}Mn_2O_7$ (b), and $La_{1.4}Sr_{0.8}Ca_{0.8}Mn_2O_7$ (c) samples after they have undergone the argon (Fig. 10) and oxygen (Fig. 11) annealing treatments. Inset in each graph presents the magnetoresistivity (MR), defined as

$$MR(\%) = \frac{\rho(H) - \rho(0)}{\rho(0)} \times 100. \quad (3)$$

In all of the ρ versus T curves, a transition from an insulating towards a metallic-like behavior is found. The values of these transitions temperatures, taken at the maximum of the $H=0$ curves and hereafter called T_ρ, are reported in Table II.

For the oxygen-annealed samples, the T_ρ values progressively reduce by increasing the Ca doping; this follows the trend reported in literature for the as-prepared samples with analogous compositions, even though with higher absolute values.[29,45] A more complex behavior is observed for the argon-annealed compounds, for which the T_ρ values, always lower with respect to T_ρ values of the as-prepared samples, reduce from 83 to 71 K going from the Ca-undoped sample to the $y=0.25$ one and increase to 100 K for the $y=0.50$ composition.

The absolute ρ values progressively reduce by increasing the Ca doping for both types of annealing. This could be directly linked to the reduction of Mn-O bond lengths as the Ca doping increases, thus making the polaron hopping easier. It is interesting to note that for the argon-annealed samples ρ varies in a very large range: the $\rho_{300\ K}$ reduces by nearly four orders of magnitude, passing from 927 Ω cm for $y=0$ to 2.2 Ω cm for $y=0.25$ and 0.9 Ω cm for $y=0.50$, while for the oxygen annealed samples we found that the ρ values, always lower with respect to the corresponding reduced samples, decrease of about one order of magnitude in the same composition range. Moreover, the width of the transition is relatively large, which may be a direct consequence of the point defects connected to the oxygen nonstoichiometry, analogous to what found in perovskite manganites.[7,8]

An upturn of resistivity at low temperature is present for all the three argon-annealed samples; this is nearly T-independent falling, irrespective to the cation doping, around 32–34 K. On the contrary, for the oxygen ones, the upturn of the resistivity at low temperature is progressively shifted from ~65 K in $La_{1.4}Sr_{1.6}Mn_2O_7$ to ~40 K in $La_{1.4}Sr_{1.2}Ca_{0.4}Mn_2O_7$ and disappears for the $La_{1.4}Sr_{0.8}Ca_{0.8}Mn_2O_7$ compound.

Coming to the MR behavior for the argon-annealed samples, we note that $La_{1.4}Sr_{1.6}Mn_2O_7$ shows a peaked MR curve with a value, at 7 T, of about 60% and centered at a temperature (~98 K) close to the T_ρ value. As usual for analogous systems, the MR peak moves to higher T as the field is increased. For $La_{1.4}Sr_{1.2}Ca_{0.4}Mn_2O_7$ the MR curve at 1 T has a peaked form with T_{peak} at about 63 K corresponding to a value of ~80% while a higher magnetic field induces a sort of *plateau* behavior with MR values ranging between 95 and 99.5% for $T<70$ K. Finally, the MR curves for $La_{1.4}Sr_{0.8}Ca_{0.8}Mn_2O_7$ show a nearly linear decrease of MR with temperature at 1 T and a peaked curve at 7 T with $T_{peak} \approx 112$ K and a MR effect of about 54%.

For the oxygen-annealed series, it can be seen that for the Ca-undoped and $y=0.25$ samples just a continuous reduction of MR with T is found while the appearance of a peak followed by an upturn towards more positive MR values is evident for the $La_{1.4}Sr_{0.8}Ca_{0.8}Mn_2O_7$ sample for all the applied fields (included $H=0.1$ T). Absolute values of the MR effect are very close for the $y=0$ and 0.25 compositions and larger for the 0.50 sample, reaching, at 7 T, a maximum value around 60% at ~75 K.

To discuss in more detail the resistivity data, we tried to model the activated part of the ρ versus T curves with the usually and widely accepted models, i.e., small polaron hopping (adiabatic and nonadiabatic) and variable range hopping (VRH), in order to extract information on the hopping energy.

For all the argon-annealed samples, a good fit in the range $1.33T_\rho \leq T \leq 320$ K was achieved considering a small polaron hopping conductivity,

$$\rho = \rho_0 T \exp(E_a/k_B T). \quad (4)$$

The hopping energies obtained are 128 meV for

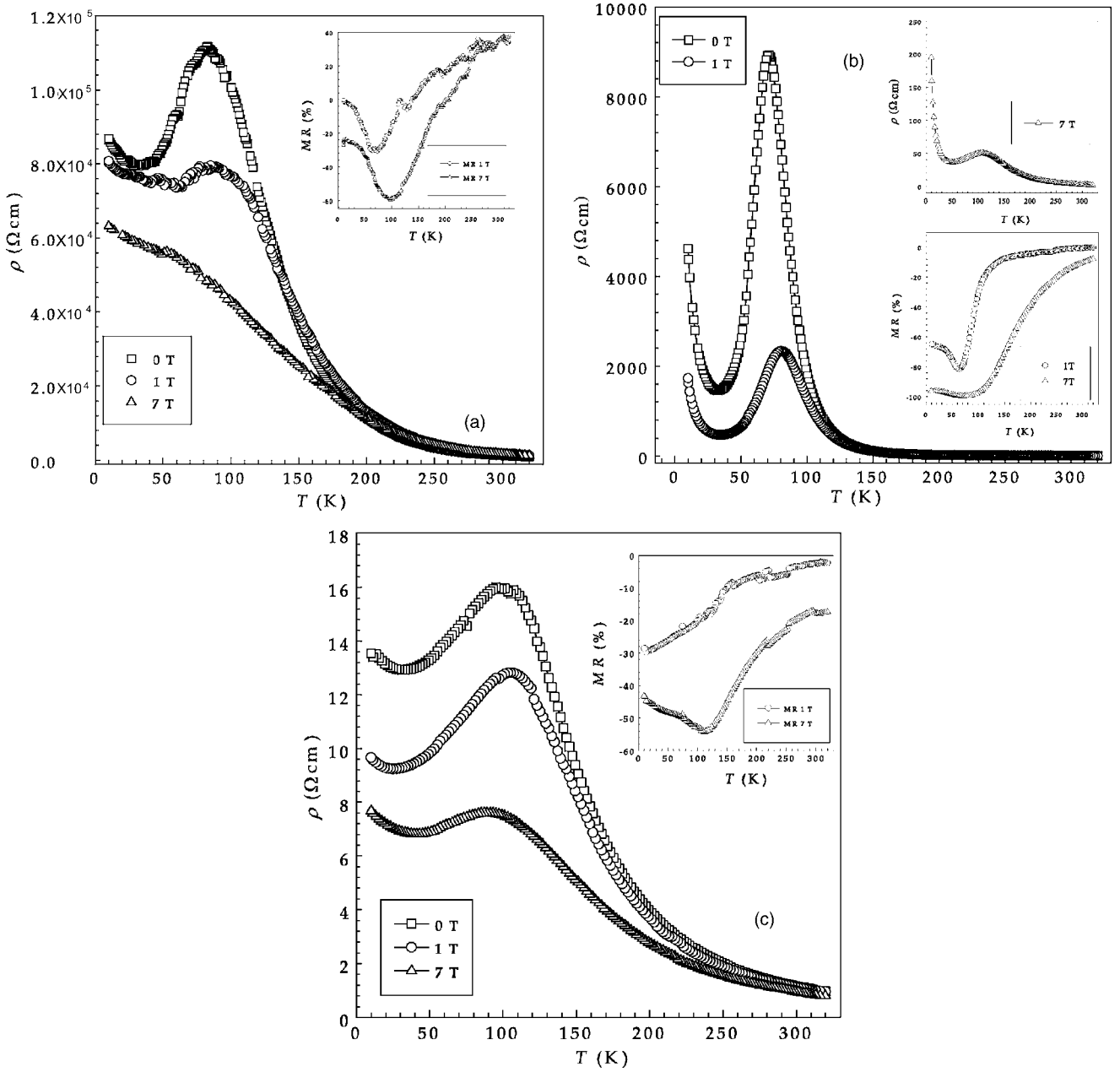

FIG. 10. Resistivity curves vs T at 0, 1, and 7 T for the argon-annealed (a) $La_{1.4}Sr_{1.6}Mn_2O_7$, (b) $La_{1.4}Sr_{1.2}Ca_{0.4}Mn_2O_7$ (in this case the 7 T ρ vs T curve is reported in the inset) and (c) $La_{1.4}Sr_{0.8}Ca_{0.8}Mn_2O_7$. In the insets: correspondent MR curves for the same samples.

$La_{1.4}Sr_{1.6}Mn_2O_7$, 75.5 meV for $La_{1.4}Sr_{1.2}Ca_{0.4}Mn_2O_7$, and 52 meV for $La_{1.4}Sr_{0.8}Ca_{0.8}Mn_2O_7$, thus indicating that carrier motion becomes progressively easier as the Ca doping increases. This is also in agreement with the reduction of resistivity values observed with the increase of calcium doping.

Since the hole doping for the three samples annealed in argon is about the same (see the XAS section for details) the reason for the easier polaron hopping could be connected to the reduction of the Jahn-Teller distortion as the Ca-doping increases, as reported in Sec. III A. We point out that the sample with the highest Ca-substitution for Sr, for which a very low c/a value is detected [5.164(3), see Table I], also displays the highest T_ρ value among the argon annealed series.

For all three samples annealed in pure oxygen, in a T range far from T_ρ, a simple power-law dependence with T was found to describe the transport behavior in the insulating phase, instead of the "usual" exponential T dependence. For the $y=0$ and $y=0.25$ compositions this could be connected to the presence of a second phase but, interestingly, the single-phase $y=0.50$ composition behaves in the same way, thus suggesting that it may be a property related to the nature of the samples themselves. A possible explanation of this result may come from the known anisotropy in the transport properties between the a-b plane and the c axis found in these materials. As reported by Kimura *et al.*[9] for the $La_{1.4}Sr_{1.6}Mn_2O_7$ the conductivity within the layers has a metalliclike trend for temperatures lower than ~270 K while it is always insulatinglike between adjacent layers. However,

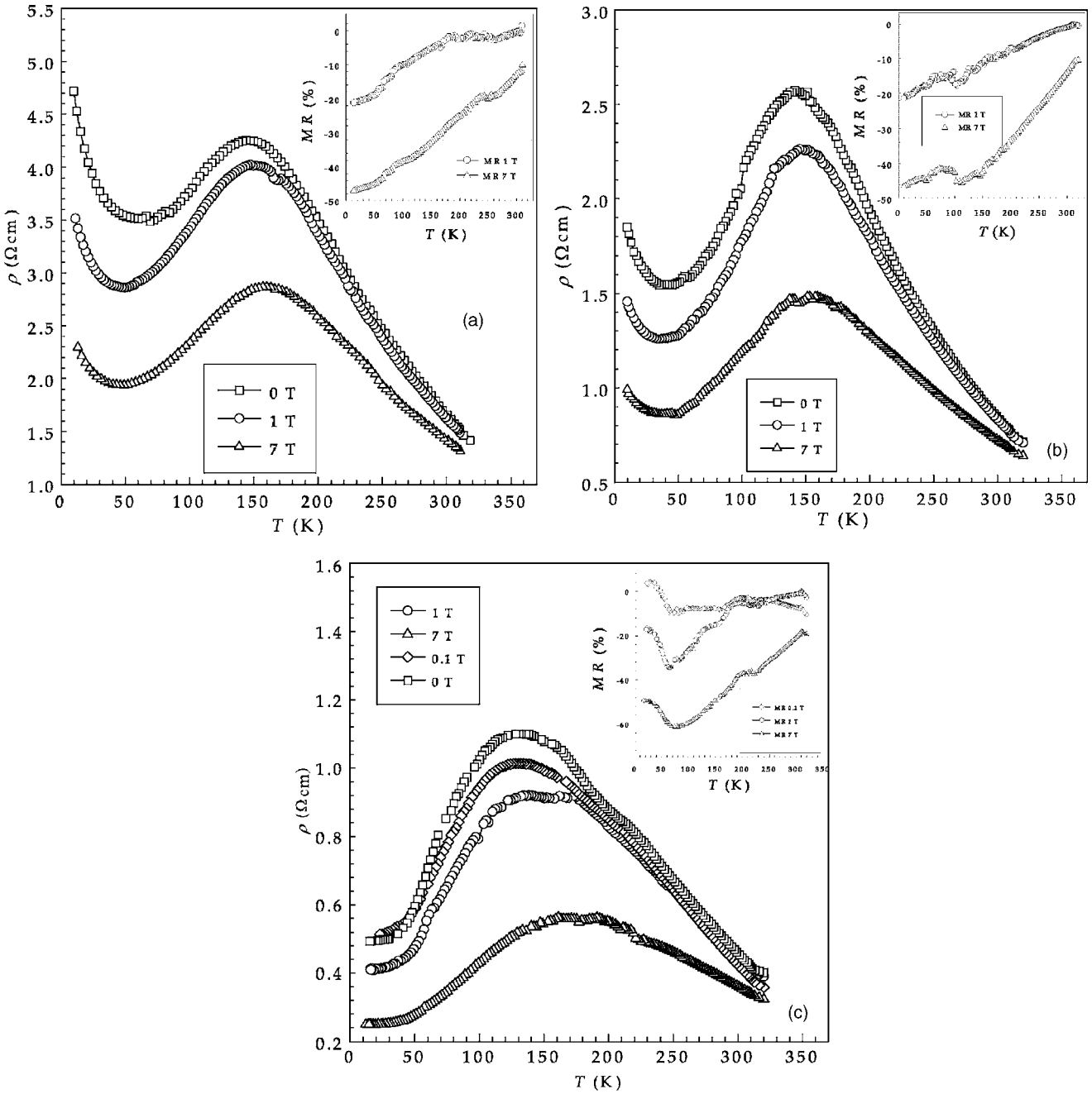

FIG. 11. Resistivity curves vs T at 0, 1, and 7 T for the oxygen-annealed (a) $La_{1.4}Sr_{1.6}Mn_2O_7$, (b) $La_{1.4}Sr_{1.2}Ca_{0.4}Mn_2O_7$, and (c) $La_{1.4}Sr_{0.8}Ca_{0.8}Mn_2O_7$ (in this case the 0.1 T ρ vs T curve is also reported). In the insets: correspondent MR curves vs T for the same samples.

for polycrystalline samples, the resistivity behavior for $T > T_\rho$ is always activated in nature. This suggests that the electrical properties are in some way influenced by the less mobile carrier transport in the out-of-plane direction.[23] So, an enhancement of the carrier motion in this direction, as presumably happens for the oxygen-annealed samples, would reduce the strong resistive contribution of the c axis hopping and lead to an overall ρ versus T trend which may not be modeled with just an activated law.

Differences in the T_ρ between the oxidized and reduced samples can be connected to the difference in the Mn average valence state: higher values for the oxygen-annealed samples (see Sec. III B) leads to higher values of the transition temperatures and the lowest T_ρ value is detected for the argon annealed $y=0.25$ composition, for which also the lowest Mn valence state is evaluated.

The different transport behavior between the two differently annealed series is also strongly related to structural effects. All the three samples annealed in pure oxygen, characterized by ρ values lower and T_ρ values higher with respect to the argon-annealed series, have a smaller unit cell with respect to those treated in argon, thanks to the higher oxidation of the Mn ions, and a c/a parameter that, on average, is lower than 5.2: the high c/a values of the argon-annealed $y=0$ ($c/a \approx 5.27$) and $y=0.25$ ($c/a > 5.22$) compositions indeed correspond to markedly higher ρ values with respect to

TABLE II. Resistivity values at 300 and at 10 K, T_ρ and T_C values, temperature, and % values of the MR peaks at 7 T and at 1 T for the oxygen (O) and argon (Ar) annealed $(La)_{1.4}(Sr_{1-y}Ca_y)_{1.6}Mn_2O_{7\pm\delta}$ (y=0, 0.25, and 0.50) samples.

Sample		$\rho_{300\ K}$ (Ωcm)	$\rho_{10\ K}$ (Ωcm)	T_ρ (K)	MR_{peak7T} T (K) and (%)	MR_{peak1T} T (K) and (%)	T_C (K)
y=0	O	1.64	4.71	146.2	-	-	56
y=0.25	O	0.71	1.84	141.5	-	-	33
y=0.50	O	0.39	0.51	134.5	74 K(62)	65 K(35)	-
y=0	Ar	927	3.2×106	83	98 K(59.7)	69 K(30.5)	53.5
y=0.25	Ar	2.2	2.5×105	71	70 K(99.5)	63 K(81.4)	30.5
y=0.50	Ar	0.9	112	100	112 K(54.3)	-	24

the other samples (see $\rho_{300\ K}$ values in Table II). In addition, we recall the Mn-O bond lengths' behavior we have shown in Fig. 9, which points out a progressive reduction of the J-T distortion as the Ca doping increases. As a consequence, the structural parameters suggest that interlayer correlations may be enhanced for all the oxidized samples. This could be also an additional reason for the different T_ρ versus y behavior for the reduced samples where, at y=0.50, an increase of T_ρ is found. Actually, among the argon-annealed samples, only the y=0.50 composition has a c/a parameter lower than 5.2.

The overall MR behavior for the considered samples is the one expected for the CMR manganites. An additional remark concerning the MR effect for y=0 and 0.25 oxygen-treated samples has to be made. The absence of peaked MR curves in both 1 and 7 T is indicative that other mechanisms in these samples may be predominant with respect to the CMR one. A smooth increase of MR effect with temperature decrease is usually connected to a tunneling magnetoresistive effect (TMR) that is enhanced as spin scattering is progressively reduced by lowering T. This is the common mechanism encountered in multilayers of FM/I/FM alternated layers (I=insulating phase; FM=ferromagnetic phase) and nanosized samples. However, from electronic microscopy the average grain size of the present samples resulted to be in the microns range, so that this origin for the observed MR effect can be ruled out. More probably, for the y=0 and 0.25 compositions, the reason for this behavior may lie in the biphasic nature of the two samples themselves possibly related to the difference in the distribution of cation vacancies and/or clustering phenomena.

D. Magnetization measurements

Figures 12 and 13 report the M versus T curves at 100 Oe for the three samples annealed in pure oxygen and argon, respectively.

The curves are characterized by a progressive enhancement of the magnetization as the temperature is reduced. In nearly all the curves, a further step rise of M/H is found at low T. The temperatures of these transitions (T_C) are reported in Table II. It can be noticed that the Ca doping (y) induces, for both the treatments, a progressive reduction of the transition temperatures as y is increased. In addition, as the Ca doping increases, also the M/H step rise at low temperature becomes relatively smaller with respect to the M/H slow enhancement from high T. This is true for both the under- and overstoichiometric samples where, for the latter series, at y=0.50, the step rise at low T has finally disappeared.

The role of cation doping on the magnetic properties of the samples may be understood within the framework of the following model according, also, to what proposed by Asano[23] and observed by Kimura.[9] At room temperature, the system is mainly composed of a paramagnetic matrix where some 2D FM in-plane correlations are already present and evolve as T is reduced towards T_C. In this region, we recall, the conductivity within the a-b planes is already metallic in nature whereas it is insulatinglike along the c axis. Due to the strong FM coupling of Mn moments starting from ~270 K and to the strong in-plane exchange interaction, the x=0.3 ($La_{2-2x}Sr_{1+2x}Mn_2O_7$) compound is considered as a quasi-two-dimensional ferromagnet (2D-FM). Together with the increase of in-plane magnetic correlations also the out-of-plane correlation strengthens with the reduction of T, i.e.,

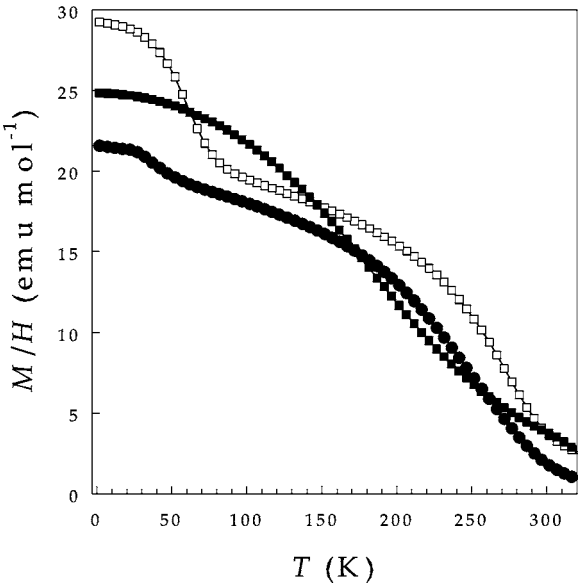

FIG. 12. Molar magnetization M/H vs T curves at 100 Oe for the oxygen-annealed $La_{1.4}Sr_{1.6}Mn_2O_7$ (white squares), $La_{1.4}Sr_{1.2}Ca_{0.4}Mn_2O_7$ (black circles), and $La_{1.4}Sr_{0.8}Ca_{0.8}Mn_2O_7$ (black squares).

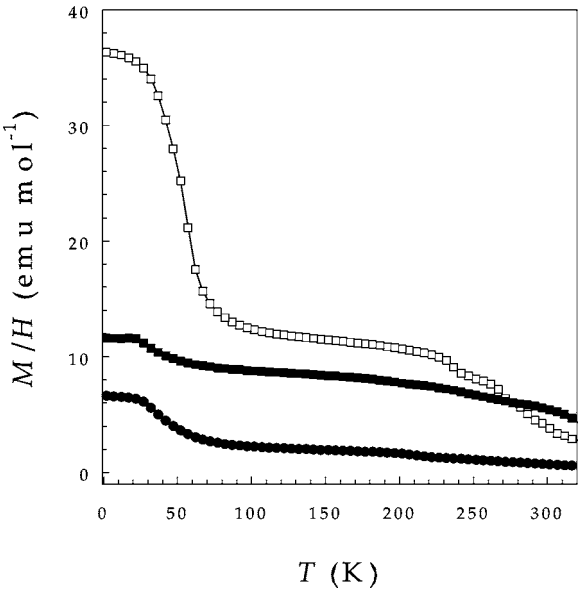

FIG. 13. Molar magnetization M/H vs T curves at 100 Oe for the argon-annealed $La_{1.4}Sr_{1.6}Mn_2O_7$ (white squares), $La_{1.4}Sr_{1.2}Ca_{0.4}Mn_2O_7$ (black circles), and $La_{1.4}Sr_{0.8}Ca_{0.8}Mn_2O_7$ (black squares).

interplane FM correlations within constituent MnO_2 bilayers. At a defined temperature, usually connected to the drop of ρ_c, a 3D-FM ordering, where the spin of neighboring MnO_2 layers are aligned along a common direction, takes place. The easy axis of the 3D spin alignment is doping dependent.[10] Finally, further reducing the temperature from T_C will allow the development of a magnetic order among MnO_2 bilayers. We also note that the 3D-FM order has been observed for a hole doping (x) around $\sim 0.30-0.40$, where fall our oxygen-annealed samples; in contrast, for the argon-annealed samples, we may not exclude the evolution of AF ordering among MnO_2 bilayers for $T<T_C$.[10] A confirmation of this comes from the observation that, moving from T_C towards lower T values, where the magnetic interaction between MnO_2 bilayers is progressively developed, by increasing the field, the molar magnetization for the Ar-annealed sample is reduced, thus suggesting that an AF interaction between MnO_2 bilayers is found, in accordance with the phase diagram developed for $La_{2-2x}Sr_{1+2x}Mn_2O_7$ when $x \leq 0.3$.

The reduction of 3D ordering temperature as Ca doping increases is connected to the progressive strengthening of the in-plane exchange interaction, J_{ab}, with respect to the out-of-plane one, J_c. This is in turn linked to the change of the orbital character of the e_g electrons. In detail, as was already pointed out in Sec. III A devoted to the x-ray diffraction analysis, the lattice constants (particularly c/a) and bond lengths' trend indicated a progressive shift of the e_g electron density from the $3z^2-r^2$ to the $3x^2-y^2$ orbitals as the Ca doping increases; accordingly, it will become *more difficult* to set up a 3D-FM ordering among MnO_2 layers and MnO_2 bilayers. However, the transfer integral of the in-plane interaction will be increased by the electron density shift, thus making the in-plane carrier hopping easier in accordance with the progressive reduction of the electrical resistivity and hopping activation energy.

This picture is able to account for the decrease of T_C with the Ca doping, but does not explain the low T_C values determined which, usually, for this doping regime, are of the order of 120–130 K (we underline that our as-prepared $La_{1.4}Sr_{1.6}Mn_2O_7$ sample has a T_C of 115 K).

However, up to now we have not considered the fact that all samples possess an oxygen stoichiometry fluctuation. As we have already put in prominence for the perovskite manganites,[7,8,24,25] the point defects connected to the δ variations are deeply effective in changing the physical properties of manganites. It is clear that even an increase of the Mn valence state, as induced by the oxygen annealing, does not lead to an increase of the magnetic transition temperatures. This has to be directly related to the cation vacancies introduced in the structure along with the oxygen overstoichiometry. Analogously, the argon-annealing treatment does not only induce a reduction of the Mn valence state but also introduce oxygen vacancies in the structure, according to

$$O_O^X \Leftrightarrow V_O^{\bullet\bullet} + 2e^- + \frac{1}{2}O_2. \tag{5}$$

We stress that the above presented picture, in which we suggest a progressive reduction of the 3D-FM ordering as the Ca doping increases, has been recently confirmed by neutron diffraction measurements.[46]

Finally, a comment about the significant difference of the T_C compared to the transition temperatures in the resistivity curves. In principle, as the FM order shifts to lower T with Ca-doping increase, we should expect also worsening effects on the transport data. But this is not the case. The only evident worsening effect caused by the Ca-doping increase is a slight reduction of the T_ρ for the oxygen overstoichiometric samples. It is clear, from the experimental evidence, that the drop in the resistivity curves, for both oxygen under- and overstoichiometric samples, is not accompanied by a 3D-FM order within planes, which, in contrast, is set up only for lower T. This might suggest that, in the present case, the transition in the resistivity is dominated by the more mobile in-plane carriers and that only for very low temperatures also the contribution from interlayer transport influences significantly the transport properties. This is also confirmed by the decrease of the ρ upturn at low T as y increases, that is when ρ_c decreases as well.

IV. CONCLUSION

In the following, we summarize the main conclusions we collected from this experimental investigation of the oxygen content variation and cation doping dependence of the $(La)_{1.4}(Sr_{1-y}Ca_y)_{1.6}Mn_2O_{7\pm\delta}$ ($y=0$, 0.25, 0.50) bilayered manganite properties:

(1) The solubility limit of the $(La)_{1.4}(Sr_{1-y}Ca_y)_{1.6}Mn_2O_7$ solid solution is around $y=0.50$; further Ca doping leads to the stabilization of the perovskite phase.

(2) Oxygen annealing induces an increase of the Mn average valence state and a transition of the crystal structure from tetragonal to orthorhombic; in addition, for $y=0$ and 0.25, a phase separation in two orthorhombic phases with

similar in-planes lattice parameters (a and b) and different c parameters is found.

(3) Thermal treatments carried out in an argon environment induce an oxygen understoichiometry in the samples; this leads, in turn, to a reduction of the Mn average valence state.

(4) The Ca doping manifests in an anisotropic behavior of the lattice parameters in the tetragonal samples; this is indicative of a change in the electronic occupancy of the e_g electrons as the doping proceeds. In addition, the Jahn-Teller distortion is reduced along with the Ca substitution.

(5) XAS analysis was carried out on all the samples on the $(La)_{1.4}(Sr_{1-y}Ca_y)_{1.6}Mn_2O_7$ solid solution. A deep analysis of the pre-edge features allowed us to propose possible correlations between the pre-edge peaks and the cation doping in the solid solution.

(6) Transport properties show a general enhancement induced by the Ca doping, as witnessed by the resistivity reduction for both the annealed series and lowering of the E_a and the IM transition temperature trend in the reduced samples. This has been directly connected to the reduction of the J-T effect promoted by the calcium doping. For the same cation composition, oxygen overstoichiometry leads to higher IM transition temperatures and lower ρ values, most probably as a consequence of the higher Mn valence state in the oxidized samples.

(7) Ca doping seems to significantly depress the FM interaction between Mn ions while improving the carrier motion; this may suggest that a strong FM coupling, as expected in the case of a double-exchange mediated transport, is not required for the hole hopping in these layered samples.

(8) Curie temperatures are reduced by increasing the Ca doping as a consequence of the progressive strengthening of the in-plane exchange interaction, J_{ab}, with respect to the out-of-plane one, J_c. This is in turn linked to the change of the orbital character of the e_g electrons.

(9) T_C for all the annealed samples is lower with respect to the as-prepared ones, even for the oxidized samples where the Mn valence state is higher; this can be connected to the strong influence on the magnetic interactions of the point defects due to the δ-variation.

(10) We finally stress that a significant difference is encountered between the T_C and T_ρ for the same sample; this sort of *uncoupling* between the two transition temperatures seems to be a direct effect of the oxygen nonstoichiometry since the same as-prepared samples presented here behaves in the "usual" way, displaying T_C and T_ρ very close each others. We propose that this effect is caused by the location of cation and oxygen vacancies introduced in the structure by the oxygen nonstoichiometry; we plan to carry out high resolution neutron diffraction measurements to try to locate these defects and correlate them to the observed effect.

ACKNOWLEDGMENTS

Financial support from the Italian Ministry of University (MIUR) through the PRIN-2004 project is gratefully acknowledged. L.M. is grateful to the Accademia Nazionale dei Lincei for financial support. Elena di Tullio is acknowledged for sample preparation. ESRF beam line BM08 (GILDA) staff is acknowledged for their support during measurement collection.

*Corresponding author. Electronic address: lorenzo.malavasi@unipv.it

[1] R. Mahendiran, S. K. Tiwary, A. K. Raychaudhuri, T. V. Ramakrishnan, R. Mahesh, N. Rangavittal, and C. N. R. Rao, Phys. Rev. B **53**, 3348 (1996).
[2] P. Schiffer, A. P. Ramirez, W. Bao, and S. W. Cheong, Phys. Rev. Lett. **75**, 3336 (1995).
[3] C. Zener, Phys. Rev. **82**, 403 (1951).
[4] A. J. Millis, P. B. Littlewood, and B. I. Shraiman, Phys. Rev. Lett. **74**, 5144 (1995).
[5] H. Röder, J. Zang, and A. R. Bishop, Phys. Rev. Lett. **76**, 1356 (1996).
[6] K. H. Ahn, T. Lookman, and A. R. Bishop, Nature **428**, 401 (2004).
[7] L. Malavasi, M. C. Mozzati, C. B. Azzoni, G. Chiodelli, and G. Flor, Solid State Commun. **123**, 321 (2002).
[8] L. Malavasi, M. C. Mozzati, P. Ghigna, C. B. Azzoni, and G. Flor, J. Phys. Chem. B **107**, 2500 (2003).
[9] T. Kimura, Y. Tomioka, H. Kuwahara, A. Asamitsu, M. Tamura, and Y. Tokura, Science **274**, 1698 (1996).
[10] T. Kimura and Y. Tokura, Annu. Rev. Mater. Sci. **30**, 451 (2000).
[11] M. Kubota, H. Fujioka, K. Hirota, K. Ohoyama, Y. Moritomo, H. Yoshizawa, and Y. Endoh, J. Phys. Soc. Jpn. **69**, 1606 (2000).
[12] C. D. Ling, J. E. Millburn, J. F. Mitchell, D. N. Argyriou, J. Linton, and H. N. Bordallo, Phys. Rev. B **62**, 15096 (2000).
[13] J. F. Mitchell, D. N. Argyriou, A. Berger, K. E. Gray, R. Osborn, and U. Welp, J. Phys. Chem. B **105**, 10731 (2001).
[14] Y. Moritomo, Y. Tomioka, A. Asamitsu, Y. Tokura, and Y. Matsui, Phys. Rev. B **51**, 3297 (1995).
[15] B. J. Sternlieb, J. P. Hill, U. C. Wildgruber, G. M. Luke, B. Nachumi, Y. Moritomo, and Y. Tokura, Phys. Rev. Lett. **76**, 2169 (1996).
[16] T. G. Perring, G. Aeppli, Y. Moritomo, and Y. Tokura, Phys. Rev. Lett. **78**, 3197 (1997).
[17] R. Osborn, S. Rosenkranz, D. N. Argyriou, L. Vasiliu-Doloc, J. W. Lynn, S. K. Sinha, J. F. Mitchell, K. E. Gray, and S. D. Bader, Phys. Rev. Lett. **81**, 3964 (1998).
[18] Y. Moritomo, A. Asamitsu, H. Kuwahara, and Y. Tokura, Nature **380**, 141 (1996).
[19] R. Seshadri, C. Martin, M. Hervieu, B. Raveau, and C. N. R. Rao, Chem. Mater. **9**, 270 (1997).
[20] J. F. Mitchell, D. N. Argyriou, J. D. Jorgensen, D. G. Hinks, C. D. Potter, and S. D. Bader, Phys. Rev. B **55**, 63 (1997).
[21] T. Okuda, T. Kimura, H. Kuwahara, Y. Tomioka, A. Asamitsu, Y. Okimoto, E. Saitoh, and Y. Tokura, Mater. Sci. Eng., B **63**, 163 (1999).
[22] P. D. Battle, M. A. Green, N. S: Laskey, J. E. Millburn, L. E. Murphy, M. J. Rosseinsky, S. P. Sullivan, and J. F. Vente, Chem.

Mater. **9**, 552 (1997).
[23] H. Asano, J. Hayakawa, and M. Matsui, Phys. Rev. B **56**, 5395 (1997).
[24] L. Malavasi, M. C. Mozzati, P. Ghigna, G. Chiodelli, C. B. Azzoni, and G. Flor, Recent Res. Dev. Phys. **4**, 545 (2003).
[25] L. Malavasi, C. Ritter, C. Tealdi, M. C. Mozzati, S. M. Islam, C. B. Azzoni, and G. Flor, J. Solid State Chem. **178**, 2042 (2005).
[26] J. A. M. van Roosmalen, E. H. P. Cordfunke, R. B. Helmholdt, and H. W. Zandbergen, J. Solid State Chem. **110**, 100 (1994).
[27] C. Ritter, M. R. Ibarra, J. M. De Teresa, P. A. Algarabel, C. Marquina, J. Blasco, J. Garcia, S. Oseroff, and S-W. Cheong, Phys. Rev. B **56**, 8902 (1997).
[28] J. E. Millburn and J. F. Mitchell, Chem. Mater. **13**, 1957 (2001).
[29] E. O. Chi, Y.-U. Kwon, J.-T. Kim, and N. H. Hur, Solid State Commun. **110**, 569 (1999).
[30] J. Rodriguez-Carvajal, Physica B **192**, 55 (1993).
[31] M. Newville, J. Synchrotron Radiat. **8**, 322 (2001).
[32] M. Crespin, J. M. Bassat, P. Odier, P. Mouron, and J. Choisnet, J. Solid State Chem. **84**, 165 (1990).
[33] M. Crespin, C. Landron, P. Odier, J. M. Bassat, P. Mouron, and J. Choisnet, J. Solid State Chem. **100**, 281 (1992).
[34] R. D. Shannon and C. T. Previtt, Acta Crystallogr., Sect. B: Struct. Crystallogr. Cryst. Chem. **B26**, 1046 (1970).
[35] D. D. Richardson, Phys. Status Solidi B **106**(1), 223 (1981).
[36] F. Bridges, C. H. Booth, M. Anderson, G. H. Kwei, J. J. Neumeier, J. Snyder, J. Mitchell, J. S. Gardner, and E. Brosha, Phys. Rev. B **63**, 214405 (2001).
[37] G. Subias, J. Garcia, J. Blasco, M. C. Sánchez, and M. G. Proietti, J. Phys.: Condens. Matter **14**, 5017 (2002), and references therein.
[38] P. Ghigna, A. Carollo, G. Flor, L. Malavasi, and G. Subias, J. Phys. Chem. B **109**, 4365 (2005).
[39] I. D. Fawcett, E. Kim, M. Greenblatt, M. Croft, and L. A. Bendersky, Phys. Rev. B **62**, 6485 (2000).
[40] I. S. Elfimov, V. I. Anisimov, and G. A. Sawatzky, Phys. Rev. Lett. **82**, 4264 (1999).
[41] Q. Qian, T. A. Tyson, C.-C. Kao, M. Croft, and A. Y. Ignatov, Appl. Phys. Lett. **17**, 3141 (2002).
[42] L. Hozoi, A. H. de Vries, and R. Broer, Phys. Rev. B **64**, 165104 (2001).
[43] M. Takahashi, J.-I. Igarashia, and P. Fulde, J. Phys. Soc. Jpn. **69**, 1614 (2000).
[44] Q. Qian, T. A. Tyson, S. Savrassov, C.-C. Kao, and M. Croft, Phys. Rev. B. **68**, 014429 (2003).
[45] M. Takemoto, A. Katada, and H. Ikawa, Solid State Commun. **109**, 693 (1999).
[46] L. Malavasi, M. C. Mozzati, C. Ritter, C. B. Azzoni, and G. Flor, Solid State Commun. **137**, 350 (2006).